Scientific Research Publishing

Graphene, 2022, 11, 1-18
https://www.scirp.org/journal/graphene
ISSN Online: 2169-3471
ISSN Print: 2169-3439

Graphene-Polymer Nanocomposites and Roll-to-Roll (R2R) Compatible Flexible Solid-State Supercapacitor Based on Graphene Nanoplatelets and Ionic Liquid-Polymer Gel

Jasper Chiguma, Eliud Mushibe, Natalya Gonopolskaya, Wayne E. Jones Jr*

Department of Chemistry and Materials Science and Engineering, Binghamton University, Binghamton, NY, USA
Email: bj95108@binghamton.edu, *wjones@binghamton.edu

How to cite this paper: Chiguma, J., Mushibe, E., Gonopolskaya, N. and Jones Jr, W.E. (2022) Graphene-Polymer Nanocomposites and Roll-to-Roll (R2R) Compatible Flexible Solid-State Supercapacitor Based on Graphene Nanoplatelets and Ionic Liquid-Polymer Gel. *Graphene*, **11**, 1-18.
https://doi.org/10.4236/graphene.2022.111001

Received: October 11, 2021
Accepted: December 21, 2021
Published: December 24, 2021

Abstract

We present the electrical and supercapacitive performance of graphene nanoplatelets in polymer nanocomposites and flexible solid state electrical double layer capacitors (EDLC) respectively. Graphene-doped poly (3,4-ethylenedioxythiophene) (PEDOT) coated polyethylene terephthalate (PET) and glass exhibited transmittance above 95% and electrical conductivity of 2.70×10^{-1} S·cm^{-1} and 9.01×10^{-1} S·cm^{-1} respectively. Graphene loaded polymethyl methacrylate (PMMA) and polystyrene (PS) nanocomposites showed electrical conductivity as high as 2.11×10^{-1} S·cm^{-1} at low loadings of 2 wt%. The use of graphene was necessitated by the need to increase the EDLC capacitance and energy density since it provides high effective surface area. The polymer gel membrane made from polyvinylidene fluoride-co-hexafluoropropylene (PVDF-co-HFP) and the Ionic Liquid (IL) 1-butyl-3-methylimidazolium hexafluorophosphate exhibited high porosity which made it suitable for use as separator in the EDLC. The highest recorded specific capacitance was 133.82 F/g which can be attributed to the porosity of the IL containing PVDF-co-HFP membrane and the large surface area of the graphene electrodes. At an operating voltage of 3.5 V the energy density was found to be 56.92 Wh·Kg^{-1}. All chemicals were research grade and were obtained from Sigma Aldrich.

Keywords

Flexible Supercapacitors, Specific Capacitance, Graphene, Roll-to-Roll, Nanocomposites, Farads

1. Introduction

Supercapacitors are promising electrochemical devices that can store energy and release it with high power capability and high current density within a short interval [1] [2]. They are therefore perfect complement for batteries or fuel cells in a myriad of applications. Among them are automobiles and high-performance portable electronics. Energy storage in supercapacitors is either by electrostatic charge accumulation on the electrode-electrolyte interface (electric double-layer capacitance) or transfer of charge to the layer of redox molecules on the surface of the electrode (pseudo-capacitance). The two storage mechanisms often work together in practical supercapacitors [3]. In order to maximize the energy density and power density that can be delivered by supercapacitor, advanced electrode materials with nanostructure and high surface area need to be developed.

Carbon, metal oxides, conducting, carbon nanotubes (CNTs) [4] and recently graphene have been aggressively studied as electrode materials for supercapacitors. Graphene is one of the most promising electrode materials for supercapacitors due to its low cost, good capacitive performance, and environmental benignity. In this work, nanostructured graphene was used as the active electrode material for the supercapacitors.

The unique properties of graphene include high thermal conductivity ~500 $W \cdot m^{-1} \cdot K^{-1}$), high electrical conductivity (10^8 $S \cdot m^{-1}$), high transparency (absorbance of 2.3%), great mechanical strength (breaking strength of 42 $N \cdot m^{-1}$ and Young's modulus of 1.0 TPa, inherent flexibility, high aspect ratio, and large specific surface area (2.63×10^6 $m^2 \cdot Kg^{-1}$) [1]. Some of the methods that have been used to extract graphene are chemical vapor deposition (CVD) of graphene on metal substrates and epitaxial growth of graphene on silicon carbide.

However, solution-based methods enable the incorporation of graphene into bulk materials and composites. The solution based methods include 1) oxidation and subsequent reduction of graphite as a pathway to isolating graphene oxide and reduced graphene oxide; 2) exfoliation of graphene in aqueous solutions using amphiphilic surfactants; 3) direct exfoliation of graphene in organic solvents; and 4) exfoliation of graphene using intercalation and electrochemical methods [5] [6] [7]. When combined with binder materials to form a nanocomposite slurry, it can be applied on a conductive substrate to form the active material of the electrode. Application of the slurry on a conductive substrate can be achieved by different coating techniques such as casting, spin-coating, doctor blading, screen printing, ink jet printing and pad printing.

Poly (3,4-ethylenedioxythiophene) (PEDOT) is one of the few intrinsically conducting polymers such as polyaniline and polypyrrole that can be blended with graphene to form conducting nanocomposites suitable for application in supercapacitors. PEDOT has great attributes such as 1) reversible doping state, it can be repeatedly doped and undoped. It is almost transparent and light blue in the oxidized state and can be easily changed into opaque and dark blue colors in the neutral state [8] [9]; 2) excellent stability, has improved chemical and ther-

mal stability, degradation occurs above 150˚C and complete decomposition above 390˚C [10], electrical conductivity almost remains unaltered after aging in environmental conditions, its stability comes from the favorable ring geometry and the electron-donating effect of the oxygen atoms at the 3,4-positions stabilizing the positive charge in the polymer backbone [11]; 3) regular structure, due to the structure of the monomer, competing polymerizations through 3- and 4-positions as in thiophene are avoided, therefore only 2,5-couplings of the ethylenedioxythiophene are expected, consequently it has fewer defects than the thiophene analogues; 4) low band-gap (higher conductivity), it has a low band gap of 1.5 - 1.6 eV [12].

The lower band-gap relative to polythiophene originating from the influence of the electron-donor ethylenedioxy groups on the energies of the frontier levels of the π system [13]. Experimental results show that after doping, PEDOT exhibits reduced absorption in the visible: the oscillator strength shifts from around 1.5 eV (lowest π-π* transition) to below 1 eV in the metallic state resulting in high electrical conductivity (up to 550 S/cm) in the doped state.

2. Experimental

2.1. Graphene-Doped PEDOT Nanocomposites

Thin films of graphene-doped poly (3,4-ethylenedioxythiophene) (PEDOT) were deposited on polyethylene terephthalate (PET) and glass. 0.1 M solutions of 3,4-ethylenedioxythiophene (EDOT) and Iron (III) chloride hexahydrate ($FeCl_3 \cdot 6H_2O$) were prepared in acetonitrile. Using bath sonication, 0.1, 1.0 and 5 wt% XG graphene nanoplates were dispersed in 0.1 M EDOT solution. After the dispersion was formed, the solution was transferred to a cold hot plate and a stir bar was inserted to maintain the dispersion. After inserting the substrates, an equal volume of 0.1 M EDOT solution was gently poured while maintaining the gentle stirring. The solution was seen to gradually turn blue. The substrates were withdrawn at 1 min intervals, rinsed in deionized (DI) water and left to dry at room temperature. The films were then characterized for electrical conductivity and transparency using a Keithley Four-point probe and UV-vis spectrophotometer respectively. Surface morphology was analyzed using the Zeiss SUPRA 55 VP high resolution scanning electron microscopy.

2.2. Graphene-Doped PMMA and PS Nanocomposites

Graphene-doped poly methyl methacrylate (PMMA) and polystyrene (PS) nanocomposites were prepared with a graphene loading of 0.1, 1.0 and 2.0 wt%. Nanocomposites were prepared at each loading using chloroform ($CHCl_3$), dimethylformamide (DMF) and tetrahydrofuran (THF). In a typical experiment, 1 g of PMMA was transferred to a vial with 10 mL of solvent. Dissolution of the polymer was achieved by magnetic stirring on a hot plate at room temperature. Separately, the required wt% of graphene was dispersed by bath sonication in an equal volume of solvent. The polymer solution and the graphene dispersion were

the mixed and further stirred and bath sonicated to achieve homogenous mixing. The graphene-polymer mixture was then poured into Teflon cups and left to dry. The films were then characterized for electrical conductivity using a Keithley Four-point probe. Surface morphology was analyzed using the Zeiss SUPRA 55 VP high resolution scanning electron microscopy. The same procedure was used to prepare samples of graphene-doped PS nanocomposites.

2.3. Graphene-Electrode Supercapacitors

Graphene particles were supplied by XG Sciences, Inc. a nanotech company focused on the manufacturing of graphene nanoplatelets and their applications in diverse fields such as energy generation and storage and composite materials. The graphene is denoted xGnP-graphite nanoplatelets and has dimensions of 1 nm × 100 nm. A slurry containing graphene and PVDF (MW = 534,000) as binder was prepared. Graphene in N-methyl pyrrolidone (NMP) was sonicated in a bath sonicator until dispersion was achieved. Separately, the PVDF was dissolved in NMP using a magnetic stir bar. The graphene dispersion and the dissolved PVDF were then mixed and further bath sonicated to achieve a homogeneous slurry of graphene-PVDF nanocomposite.

Flexible aluminum sheets were stretched on large glass plates. Part of the slurry was transferred to the aluminum and ran over by a doctor blade. A uniform continuous layer of slurry was formed. The glass plate with the graphene slurry aluminum was transferred to an oven at 80˚C and left to dry overnight. Pieces of the graphene coated aluminum were cut measuring one square inch. The mass of the coating on each piece was determined by subtraction. The ionic liquid (IL) 1-butyl-3-methylimidazolium hexafluorophosphate and the polymer Polyvinylidene Fluoride-co-Hexafluoropropylene (PVDF-co-HFP) M_w = 400,000 and M_w > 400,000 were used in the mass ratio PVDF-co-HFP/IL = 20/80 to prepare electrode separators. The polymer was dissolved in acetone using an oil bath at 50˚C. Upon dissolution, the ionic liquid was injected into the solution. After further mixing, the solution was then drop-cast on glass slides and left to dry.

The supercapacitors were assembled by putting two symmetrical electrodes together separated by a flexible PVDF-co-HFP/IL polymer gel membrane. Conductive copper tape strips from Ted Pella were attached to each Al electrode to serve as current collectors. This was followed by sandwiching the supercapacitor between two glass plates and then applying quick setting glue on the edges to seal it. The glue was obtained from Tedd Pella. The supercapacitors were left overnight to allow the glue to set and then voltage-time graphs were obtained using 4200-SCS Semiconductor Parameter Analyzer.

3. Results and Discussion

3.1. Graphene-Doped PEDOT Nanocomposites

Figure 1(a) shows pictures of pristine PEDOT thin films on glass. During the *in-situ* polymerization of 3,4-ethylenedioxythiophene to poly (3,4-ethylenedioxythiophene),

the glass slides were withdrawn at 1 minute interval up to 5 minutes. The letter *p* stands for pristine, indicating that the polymerization was done in the absence of graphene. It can be seen that the PEDOT films got darker with increase in polymerization time. At short polymerization time the PEDOT film is sky-blue in color and transparent. Figure 1(b) shows the films that were formed when polymerization took place in the presence of 0.1 wt% graphene. The slides were withdrawn at 1 minute interval up to 5 minutes. It can be seen that the films get darker as polymerization time increases from one to five minutes. Figure 1(c) and Figure 1(d) show PEDOT films that were deposited on glass in the presence of 1 wt% and 5 wt% graphene respectively and withdrawn from the polymerization vessel at 1 minute intervals up to 5 minutes. Figure 1(e) shows PEDOT films on PET that were deposited in the presence of 0.1 wt% graphene and Figure 1(f) is an SEM image of graphene doped PEDOT.

Figure 2 shows the transmission spectra of 1 wt% graphene-doped PEDOT nanocomposite films that were obtained after *in-situ* polymerization for 1 to 5 minutes. It can be seen that the films maintain high transparency of at least 90% in the visible region at around 450 nm wavelength. The films maintain high transparency after doping with graphene.

The electrical conductivity of the nanocomposite films on both glass and PET are shown in Table 1 and plotted in Figure 3. The general trend in electrical conductivity shows an initial increase followed by a decrease as the percentage loading approaches 5 wt%. As the polymerization progressed it was noticed that at around 5 minutes the polymer began to crush into the solution. This crushing lessens the amount of polymer that is deposited on the substrate.

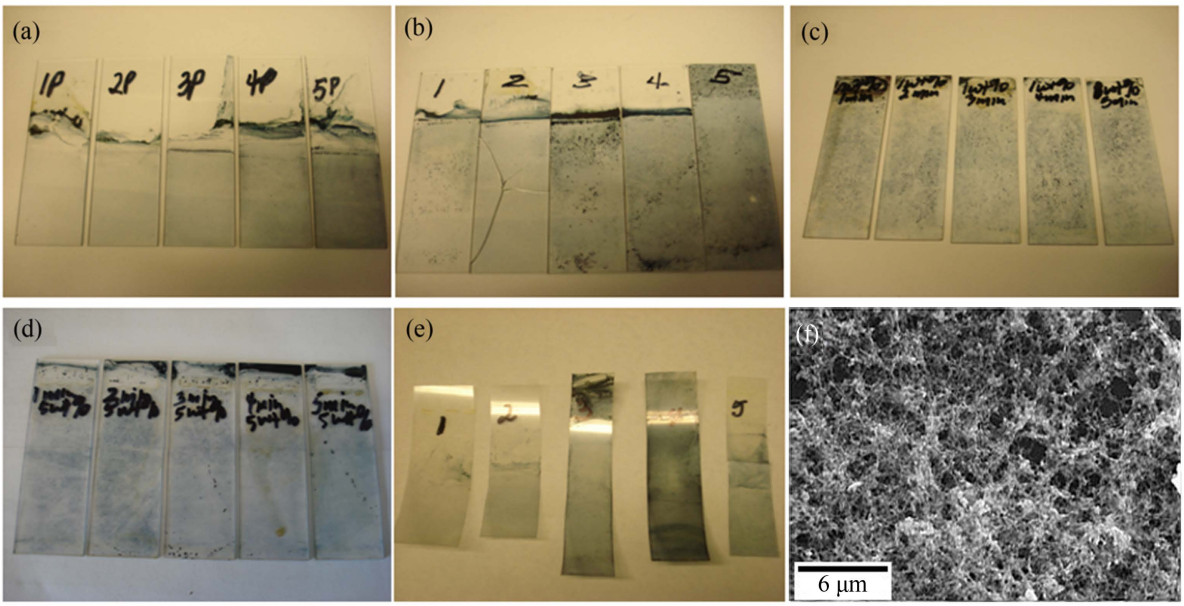

Figure 1. (a) PEDOT film on glass; (b) 0.1 wt% graphene-doped PEDOT on glass; (c) 1 wt% graphene-doped PEDOT on glass; (d) 5 wt% graphene-doped PEDOT on glass; (e) 0.1 wt% graphene-doped PEDOT on PET; (f) SEM of graphene doped PEDOT film on glass.

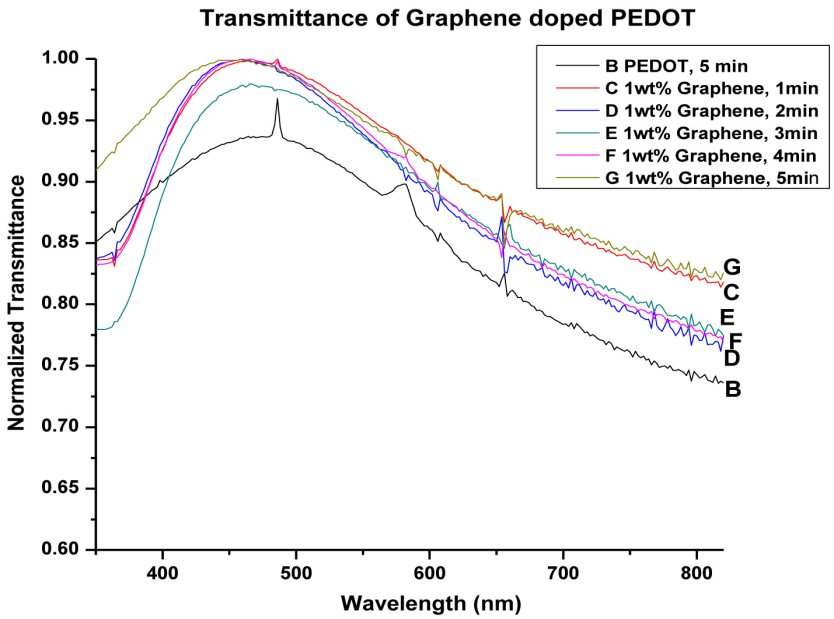

Figure 2. Transmittance of graphene-doped PEDOT nanocomposite films.

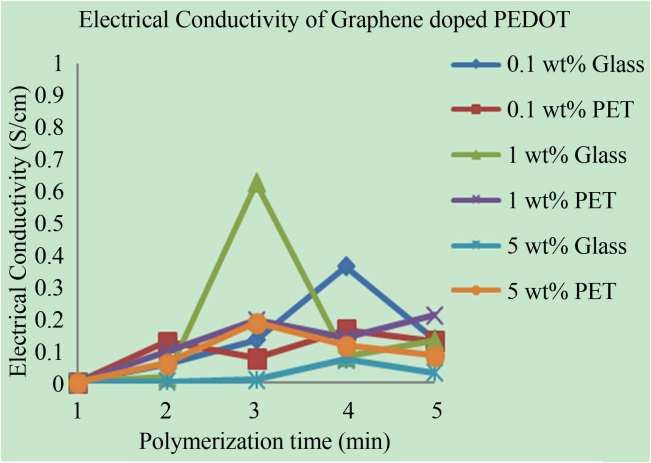

Figure 3. Electrical conductivity of PEDOT doped with 0.1, 1 and 5 wt% graphene on glass and PET.

Table 1. Electrical conductivity of graphene-doped PEDOT on glass and PET Electrical Conductivity (S/cm).

Polymerization time	0.1 wt% xGnP	0.1 wt% xGnP	1.0 wt% xGnP	1.0 wt% xGnP	5 wt% xGnP	5 wt% xGnP
Minutes	Glass	PET	Glass	PET	Glass	PET
1	0.0567	0.128	0.0176	0.0982	0.00199	0.0599
2	0.134	0.0763	0.626	0.194	0.00772	0.188
3	0.363	0.0763	0.0802	0.142	0.0726	0.116
4	0.135	0.131	0.131	0.211	0.0302	0.0837
5	0.903	0.108	0.109	0.270	0.224	0.0509

3.2. Graphene-Doped PMMA and PS Nanocomposites

Figure 4 shows the SEM images of graphene-based nanocomposites that were made from PMMA and PS and graphene at different loadings of graphene. The solvents chloroform, dimethylformamide and tetrahydrofuran were used in the preparation of each nanocomposite. These solvents have different solubility parameters which tend to affect the way they interact with each polymer and the filler and consequently affect the morphology of the resultant nanocomposite [14]. The solution-mixing method for synthesizing nanocomposites has been applied for both non-conducting polymers such as poly (vinyl alcohol), poly (methyl methacrylate), poly (vinylidene fluoride), polystyrene and polycarbonate and conducting polymers such as sulfonated poly (phenylene ethylene), poly (3-hexylthiophene-2,5-diyl), and poly (3,4-ethylenedioxythiophene) [15]-[25].

The nanocomposites that were prepared using PMMA and DMF were found to have a porous morphology as shown in the SEM images in Figure 4(a) and (b). This porous morphology makes them suitable for use in supercapacitors as electrode separators. These pores are capable of holding electrolyte and function in the same way as the PVDF-co-HFP that was used as separators in the supercapacitors that are described in the later section of this work. Table 1 shows the variation of electrical conductivity of the nanocomposites of PMMA and PS loaded with graphene with increasing loading of graphene.

Figure 5 shows the plots of the electrical conductivity data that are shown in Table 2. While all the nanocomposites show an increase in electrical conductivity with increasing graphene loading, the nanocomposites that were prepared using DMF as a solvent, show higher electrical conductivity at each loading.

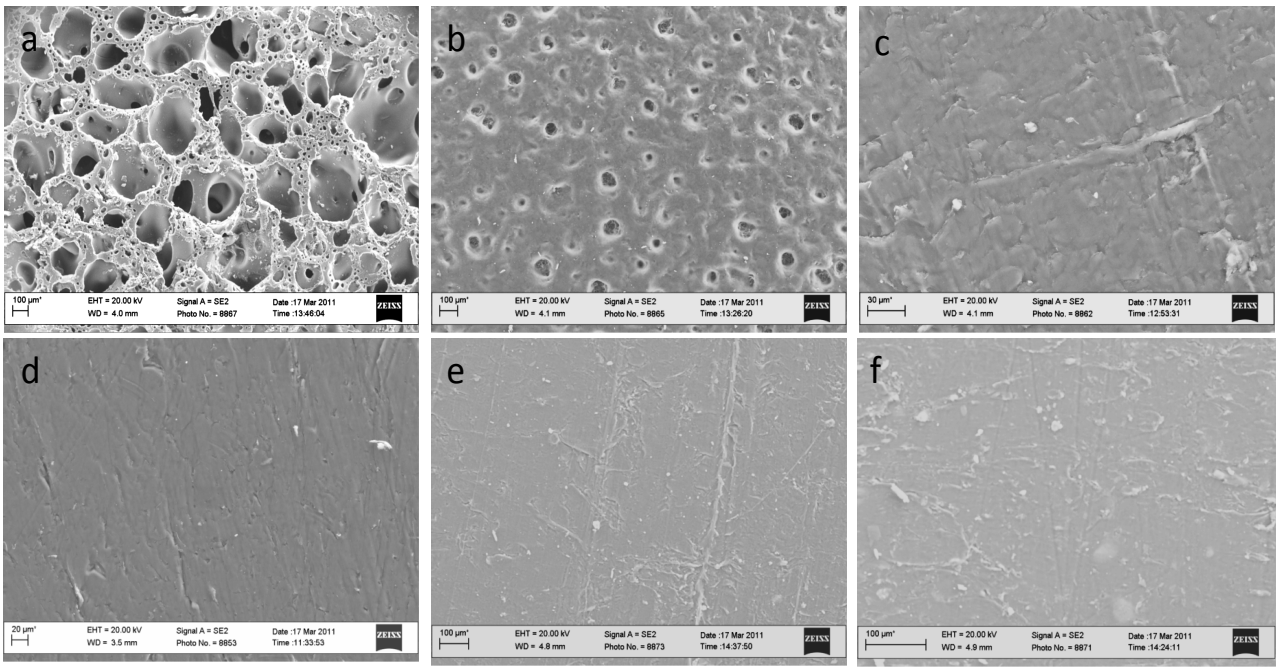

Figure 4. SEM images. (a) Cross-section 0.1 wt% xGnP-PS/DMF; (b) Surface 0.1 wt% xGnP-PMMA/DMF; (c) Surface 0.1 wt% xGnP-PS/$CHCl_3$; (d) Surface 0.1 wt% xGnP-PMMA/$CHCl_3$; (e) Surface 0.1 wt% xGnP-PS/THF; (f) Surface 0.1 wt% xGnP-PMMA/THF.

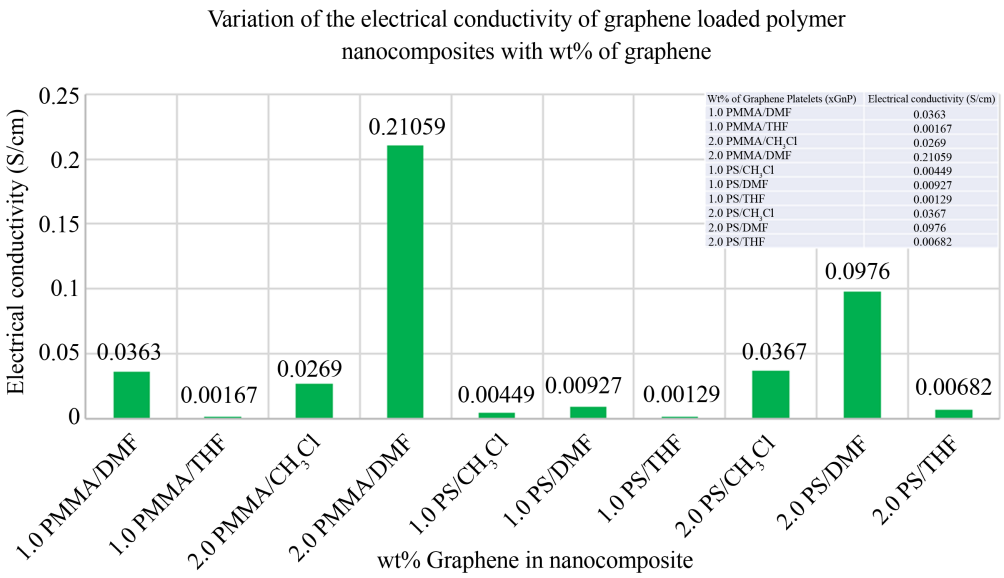

Figure 5. Plots of the electrical conductivity of graphene loaded PMMA and PS nanocomposites.

Table 2. Electrical conductivity of graphene loaded PMMA and PS nanocomposites.

Nanocomposite	Electrical Conductivity/Scm^{-1}
PMMA/0.1 wt% Graphene/$CHCl_3$	-
PMMA/0.1 wt% Graphene/DMF	-
PMMA/0.1 wt% Graphene/THF	-
PMMA/1.0 wt% Graphene/$CHCl_3$	-
PMMA/1.0 wt% Graphene/DMF	3.63×10^{-2}
PMMA/1.0 wt% Graphene/THF	1.67×10^{-3}
PMMA/2.0 wt% Graphene/$CHCl_3$	2.69×10^{-2}
PMMA/2.0 wt% Graphene/DMF	0.21059
PMMA/2.0 wt% Graphene/THF	-
PS/0.1 wt% Graphene/$CHCl_3$	-
PS/0.1 wt% Graphene/DMF	-
PS/0.1 wt% Graphene/THF	-
PS/1.0 wt% Graphene/$CHCl_3$	4.49×10^{-3}
PS/1.0 wt% Graphene/DMF	9.27×10^{-3}
PS/1.0 wt% Graphene/THF	1.29×10^{-3}
PS/2.0 wt% Graphene/$CHCl_3$	3.67×10^{-2}
PS/2.0 wt% Graphene/DMF	9.76×10^{-2}
PS/2.0 wt% Graphene/THF	6.82×10^{-3}

3.3. Graphene-Electrode Supercapacitors

Figures 6(a)-(c) show the SEM images of the graphene nanocomposite active layer, the assembly process of the EDLC and the assembled EDLC respectively.

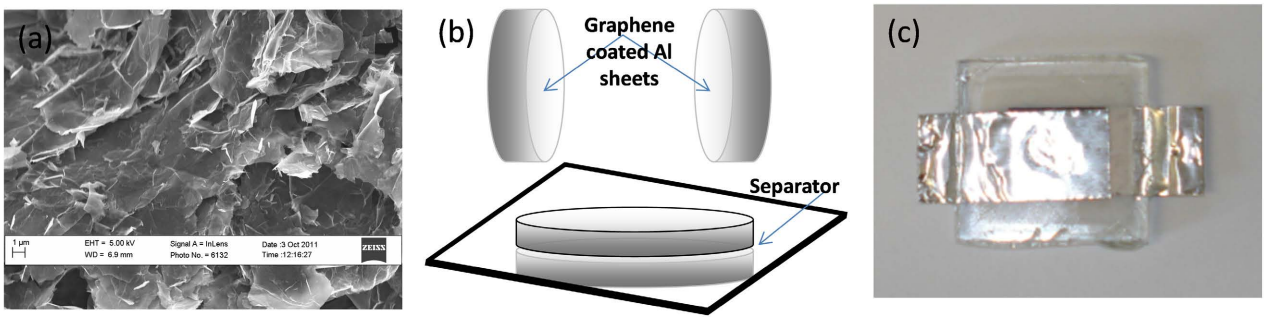

Figure 6. (a) SEM of graphene nanocomposite; (b) Assembly of EDLC; (c) Assembled EDLC.

In **Figure 6(a)**, it can be seen that the graphene layers lie overlapping each other. A relatively smooth surface with a large surface area is thus formed.

3.4. Doctor Blading

The doctor blade coating technique works by placing a sharp blade at a fixed distance from the substrate surface that is to be coated usually 10 - 500 μm [26]. The coating solution is then placed in front of the blade that is then moved linearly across the substrate leaving a thin wet film after the blade. The final wet thickness of the film is ideally half the gap width but may vary due to the surface energy of the substrate, the surface tension of the coating solution and the viscosity of the coating solution. It also depends on the meniscus formed between the blade and the wet film on the trailing edge of the blade, which is related to the shear field (proportional to the speed of the blade/knife). The final dry thickness of the coated film, d, can be calculated from the following empirical relationship:

$$d = \frac{1}{2} g\left(c/\rho\right)$$

where g is the gap distance between the blade and the substrate in cm, c is the concentration of the solid material in the ink in g·cm^{-3} and, ρ is the density of the material in the final film in g·cm^{-3}.

Doctor blading allows for the formation of films with a well-defined thickness. It is quite parsimonious and with some practice the loss of coating solution can be minimized such that less than ~5% is lost. Doctor blading is easily transferable to an R2R coating environment and is in this context known as knife-over-edge coating (*vide supra*). In this case the knife is stationary and the web is moving. The knife is suitably used in conjunction with an ink bath positioned in front of the knife with respect to the direction of movement of the web. **Figure 7** shows the film that was formed from graphene with binder after being deposited on aluminum.

3.5. PVDF-Co-HFP Copolymer and Ionic Liquid 1-Butyl-3-Methylimidazolium Hexafluorophosphate

Depending on their HFP percentages PVDF-co-HFP copolymers can behave as

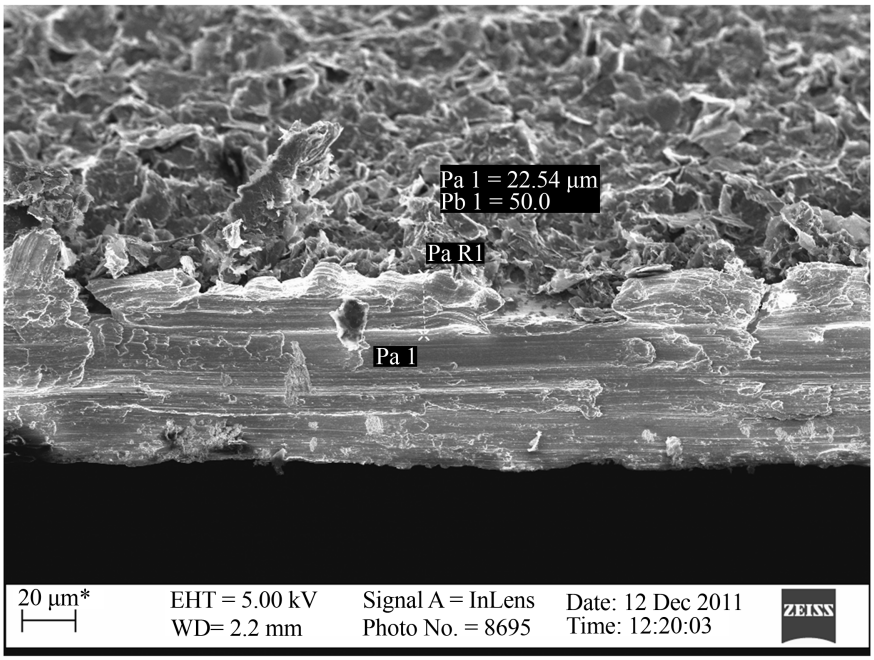

Figure 7. FE-SEM cross-section image of graphene active material on Al.

thermoplastics, elastomers or thermoplastic elastomers. When they are crosslinked, they have high thermostability and exhibit improved mechanical properties, and are resistant to oils, fuels, chemicals making them suitable for hostile environments. PVDF-co-HFP copolymers can serve as host for liquid electrolytes for applications in energy storage devices such as lithium-ion batteries. It has been shown that ionic conductivity of polymeric gel electrolytes can be increased by embedding liquid electrolyte in the pores or by inserting nanoparticles or ionic liquid in the pores of the PVDF-co-HFP copolymer [27] [28] [29].

Ionic liquids (ILs) are molten salts at room temperature and entirely composed of cations and anions. The nature of these ions determines the chemical, electrochemical and physical properties of the ILs. These molten salts have low vapor pressure and are characterized by high boiling/decomposition points even at 400˚C. They are considered green solvents because since they are free of toxic and flammable organic solvents and are capable of operating at high temperatures. They provide an opportunity to develop safe green high voltage supercapacitors. These molten salts are resistant to electrochemical reduction and oxidation and they have wide electrochemical stability window (ESW) [30] [31] [32] [33].

The hydrophobicity of these salts, which depends on the properties of the ions composing the IL, is of primary importance in guaranteeing a high life cycle of supercapacitors based on ionic liquids. The hydrophobicity is determined by the substituents of the cations and decreases in the order $CF_3CO_2^-$, $CH_3CO_2^-$ (hydrophilic) > $CF_3SO_3^-$, BF_4^- > PF_6^-, $(CF_3SO_2)_2N^-$ (hydrophobic). The ionic liquids mainly studied for supercapacitors are imidazolium, pyrrolidinium, and asymmetric, aliphatic quaternary ammonium salts of anions like tetrafluorobo-

rate (BF_4^-), trifluoromethanesulfonate (Tf), bis (trisfluoromethanesulfonyl) imide ($TFSI^-$), bis (fluorosulfonyl66) imide (FSI^-) and hexafluorophosphate (PF_6^-), and all have an ESW wider than that of the conventional electrolyte at room temperature [34] [35] [36]. **Figure 8** shows the SEM images of the polymer gel that was prepared by blending PVDF-co-HFP copolymer and Ionic Liquid 1-butyl-3-methylimidazolium hexafluorophosphate. It can be seen from these images that the polymer gel membrane is highly porous.

3.6. Electrochemical Characterization

Figure 9 shows the voltage-time graph that was obtained for an electrochemical double layer capacitor that had the following compositions: 5 wt% PVDF binder and 95% graphene on aluminum foil.

The capacitance (C) of the supercapacitor was calculated by measuring the slope of the charging curve before the onset of the Faradaic current i_F, *i.e.* before $i_F > 0$ [37]. The slope is equal to the inverse of the capacitance, *i.e.* slope = $1/C$ $\Rightarrow$ $C = 1/\text{slope} = 1/(\mathrm{d}V/\mathrm{d}t)$. Specific capacitance ($C_{sp}$) is the capacitance per unit mass for one electrode. Assuming a symmetric electrochemical capacitor, that is, a capacitor whose charge storage mechanism consists of storing charge in the electrical double layers at the electrode/electrolyte interface unlike an

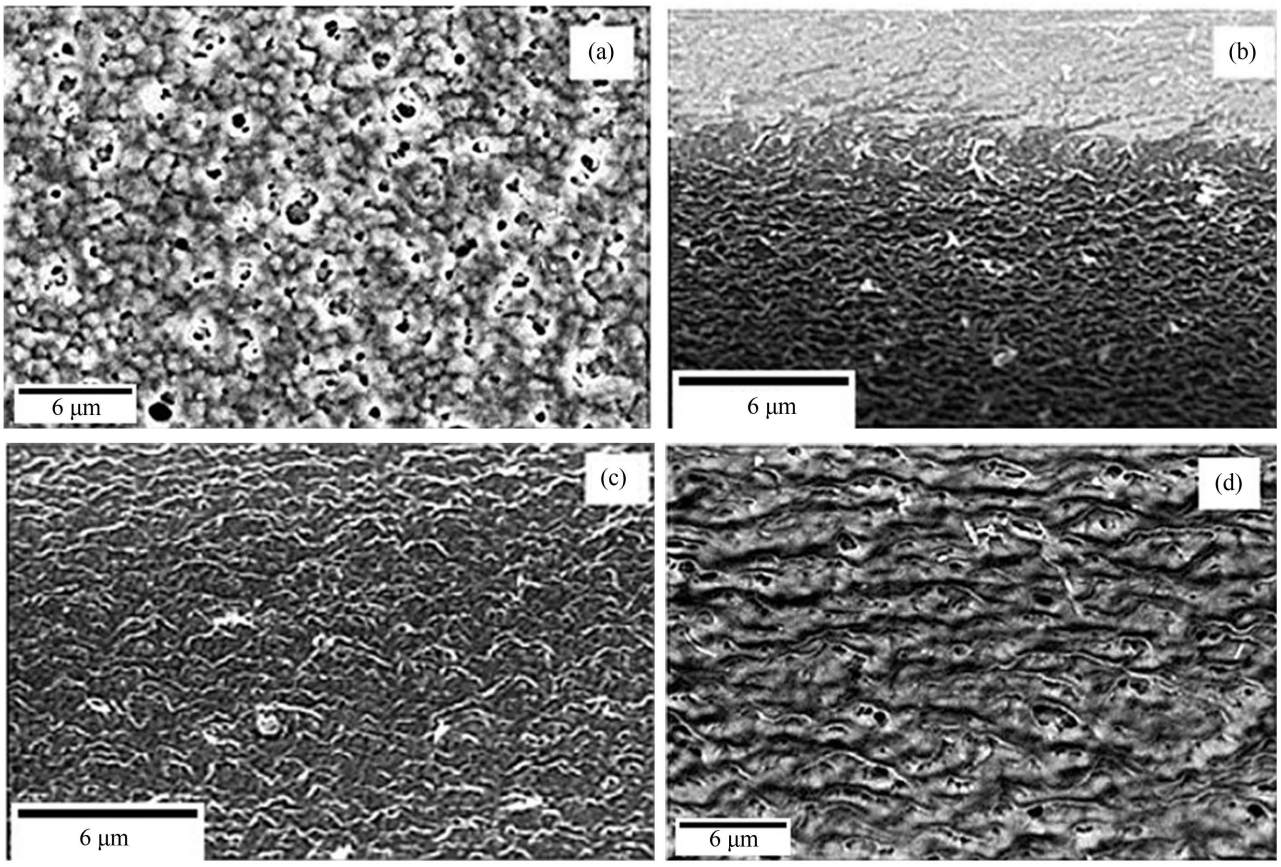

Figure 8. SEM images of polyelectrolyte separator of composition PVDF-co-HFP/IL = 20/80. (a) Surface, (b), (c) and (d) Cross-section.

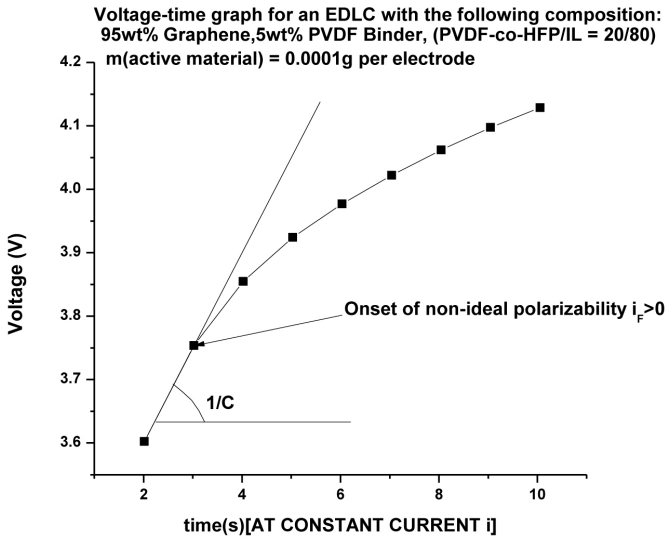

Figure 9. Voltage-time charging graph at constant current of a supercapacitor with 5 wt% PVDF binder and polyelectrolyte separator of composition PVDF-co-HFP/IL = 20/80.

asymmetric which utilizes both electrical double layers and Faradaic redox processes to store energy, the specific capacitance of each two electrode supercapacitor was calculated according to the following formula [38] [39]:

$$C_{sp} = 2 \times I / \left[\left(\mathrm{d}V/\mathrm{d}t \right) \times m \right]$$

where I is the constant current (0.001 Amp), $\mathrm{d}V/\mathrm{d}t$ is the slope (0.1494) of the charging curve, and m is the mass of active material on one electrode (0.0001 g). $\mathrm{d}V/\mathrm{d}t$ was calculated from the slope obtained by fitting a straight line to the charging curve before the onset of the Faradic current. The formula is arrived at starting as follows:

$$\begin{aligned} C_{sp} &= \left\{ \left[I / \left(\mathrm{d}V/\mathrm{d}t \right) \right] \left[1/m_1 + 1/m_2 \right] \right\} \\ &= \left\{ \left[I / \left(\mathrm{d}V/\mathrm{d}t \right) \right] \left[2/m \right] \right\} \quad \text{assuming } m_1 \approx m_2 \end{aligned}$$

When the values of I, $\mathrm{d}V/\mathrm{d}t$ and m were substituted the value 66.93 was obtained which after being multiplied by 2 gave a C_{sp} value of 133.86 F/g. The factor of 2 comes from the fact that the total capacitance measured from the test cells is the addition of two equivalent single-electrode capacitors in series. The energy density (E) was calculated using the following formula:

$$E_{\text{density}} = 1/8 C_{sp} V_{\max}^2$$

where $V_{\max}$ is the maximum voltage. At a maximum voltage of 3.5 V and specific capacitance of 133.86 F/g, the energy density of 56.92 Wh·kg^{-1}, was achieved.

Figure 10 shows the V-t graphs that were obtained for supercapacitors that were constructed with a slurry composed of 5% binder, 95% graphene, the polymer gel separator membrane composed of the copolymer PVDF-co-HFP and the ionic liquid 1-butyl-3-methylimidazolium hexafluorophosphate in the ratio 20/80. The molecular weight (M_w > 400,000) of the PVDF-co-HFP was greater than 400,000. It can be seen that the supercapacitors were stable above 3.0 V.

The specific capacitance values were calculated by drawing a tangent to the curves near the beginning of the curves and finding the slope. These values were further confirmed by differentiating the voltage data with respect to time (dV/dt) and taking the first value. The results were found to agree and are tabulated in Table 3. Figure 11 shows the V-t graphs of supercapacitors that were prepared with the same composition as those in Figure 10 except that the molecular weight (M_w) of the copolymer PVDF-co-HFP was 400,000. The specific capacitances of these supercapacitors are tabulated in Table 4.

In each case the thickness of active layer film was increased which is reflected in the increase in mass. In both cases the results indicate that the increase in film thickness and consequently the increase in mass of the active material results in a decrease of specific capacitance. This trend is shown on the plots in Figure 12 and the data is summarized in Table 5.

Table 3. Specific capacitances (C_{sp}) of the supercapacitors with the V-t graphs shown in Figure 10.

Mass of active material per electrode/g	Slope from graph	$C_{sp} = 2 \times I/[(\mathrm{d}V/\mathrm{d}t] \times m$	$\mathrm{d}V/\mathrm{d}t$	$C_{sp} = 2 \times I/[(\mathrm{d}V/\mathrm{d}t] \times m$
0.00010	0.1494	133.82	0.151	132.70
0.00015	0.2927	45.54	0.294	45.42
0.00025	0.2338	42.78	0.239	41.84

Table 4. Specific capacitances (C_{sp}) of the supercapacitors with the V-t graphs shown in Figure 11.

Mass of active material per electrode/g	Slope from graph	$C_{sp} = 2 \times I/[(dV/dt] \times m$	dV/dt	$C_{sp} = 2 \times I/[(dV/dt] \times m$
0.00010	0.2901	68.94	0.299	66.91
0.00015	0.1880	70.92	0.191	69.80
0.00025	0.2368	33.78	0.240	33.33

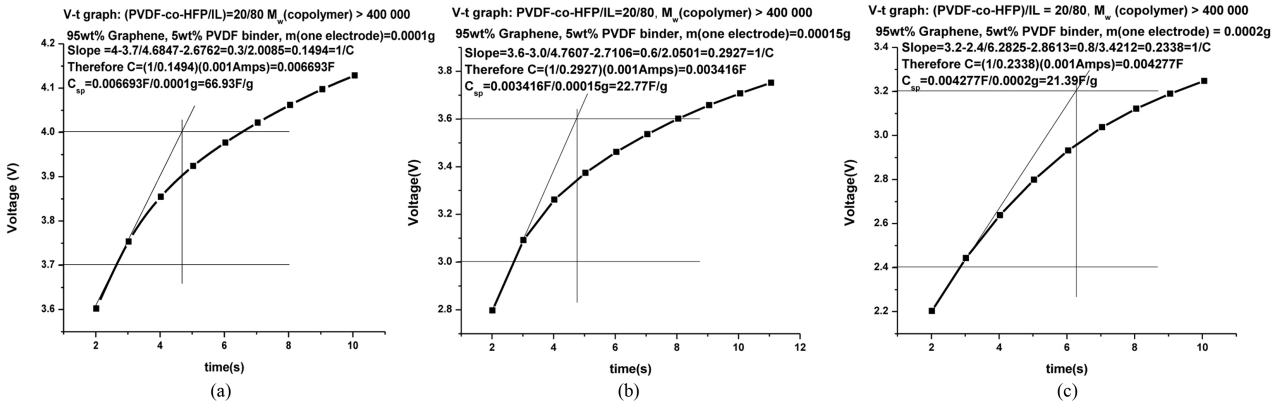

Figure 10. V-t graphs of supercapacitors at 5 wt% binder, PVDF-co-HFP (M_w > 400,000)/IL in the mass ratio 20/80 and increasing mass of active electrode (a) 0.0001 g; (b) 0.00015 g; (c) 0.00025 g.

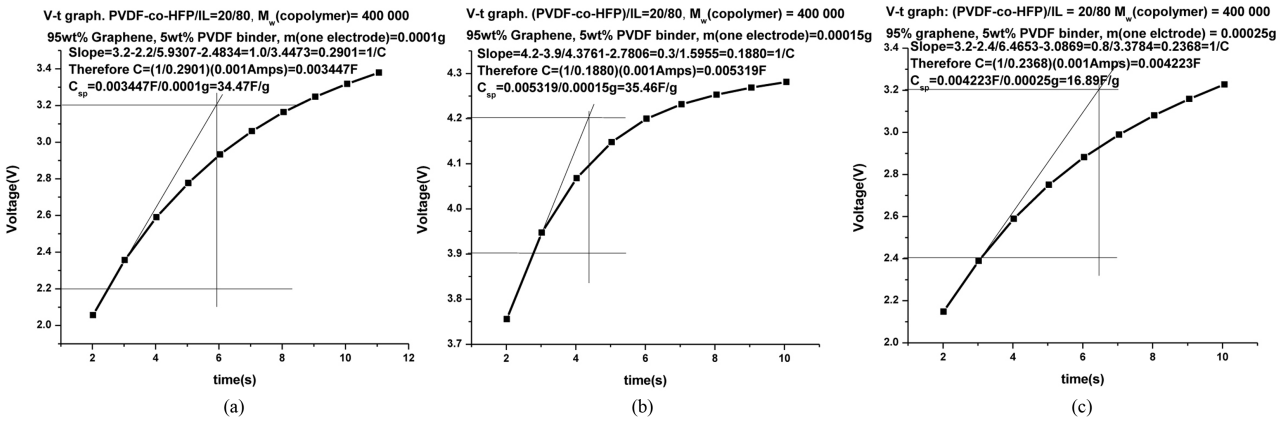

Figure 11. V-t graphs of supercapacitors at 5 wt% binder, PVDF-co-HFP (M_w = 400,000)/IL in the mass ratio 20/80 and increasing mass of active electrode (a) 0.001 g; (b) 0.00015 g; (c) 0.00025 g.

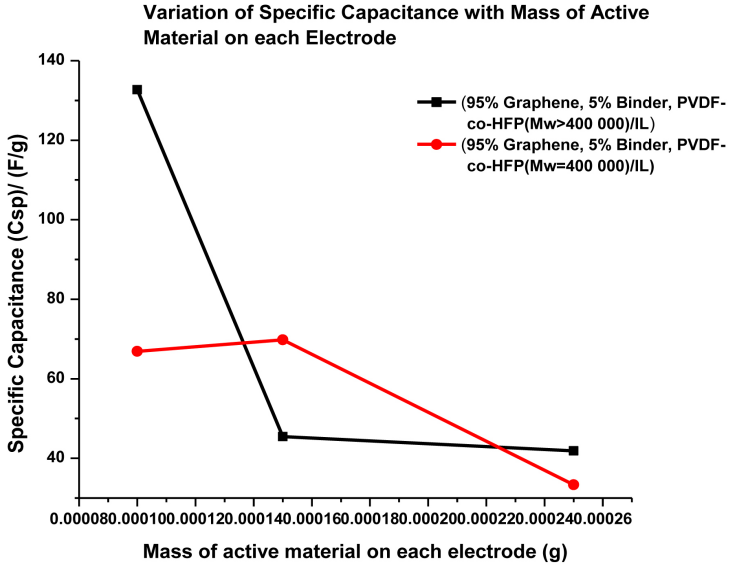

Figure 12. Variation of specific capacitance (C_{sp}) with mass of active material on each electrode.

Table 5. Variation of specific capacitances (C_{sp}) of the supercapacitors with mass of active material on each electrode plotted in **Figure 12**.

Mass of active material per electrode/g	C_{sp}, M_w (PVDF-co-HFP) > 400,000	C_{sp}, M_w (PVDF-co-HFP) = 400,000
0.00010	133.82	132.70
0.00015	45.54	45.42
0.00025	42.78	41.84

4. Conclusion

Graphene was successfully used as filler in the polymers PEDOT, PMMA and PS resulting in the formation of graphene/polymer nanocomposites. The PEDOT

nanocomposites were found to have high transparency even after doping with graphene. The electrical conductivity was also found to increase making the nanocomposite a good candidate for application as a transparent conducting electrode in solar cell and electrode material for supercapacitors. The morphology of the PMMA and PS nanocomposites was found to vary depending on the solvent that was used. It was found that the use of DMF as a solvent in the preparation of PMMA and PS nanocomposites resulted in a porous structure. Such a structure has the potential for application as a separator in supercapacitors because the pores could hold electrolyte. Flexible supercapacitors with electrodes made from graphene/binder slurry and the copolymer PVDF-co-HFP/ionic liquid gel as separator were successfully assembled. The specific capacitance was found to vary with the thickness or mass of the active material at each electrode. The supercapacitors were found to be stable up to at least 3.0 V operating voltage.

Acknowledgements

We would like to acknowledge XG Sciences, Inc. for supplying the graphene nanoplatelets. Thanks to Binghamton University Advanced Analytical and Diagnostic Laboratory for making available some of the instruments that were used for materials characterization. Thanks to Binghamton University Department of Physics for making available the 4200-SCS Semiconductor Parameter Analyzer that was used to obtain voltage-time graphs data.

Conflicts of Interest

The authors declare no conflicts of interest regarding the publication of this paper.

References

[1] Cai, X., Sun, K., Qui, Y. and Jiao, X. (2021) Recent Advances in Graphene and Conductive Polymer Composites for Supercapacitor Electrodes: A Review. *Crystals*, **11**, 947-962. https://doi.org/10.3390/cryst11080947

[2] Jakube, P., Bartusek, S., Dvoracek, J.J., Sedajova, V., Kupka, V. and Otyrpka, M. (2021) Flax-Derived Carbon: A Highly Durable Electrode Material for Electrochemical Double-Layer Supercapacitors. *Nanomaterials*, **11**, 2229-2241. https://doi.org/10.3390/nano11092229

[3] Mirzaeian, M., Abbas, Q., Hunt, M.R.C. and Hall, P. (2020) Pseudocapacitive Effect of Carbons Doped with Different Functional Groups as Electrode Materials for Electrochemical Capacitors. *Energies*, **13**, 5577-5597. https://doi.org/10.3390/en13215577

[4] Bates, J., Markoulidis, F. and Lekakou, C. (2021) Design of Porous Carbons for Supercapacitor Applications forDifferent Organic Solvent-Electrolytes. *Journal of Carbon Research*, **7**, 15-31. https://doi.org/10.3390/c7010015

[5] Diez-Pascal, A.M. (2021) Development of Graphene-Based Polymeric Nanocomposites: A Brief Overview. *Polymers*, **13**, 2978-3002. https://doi.org/10.3390/polym13172978

[6] Perumal, S., Atchudan, R. and Cheong, I.W. (2021) Recent Studies on Dispersion of

Graphene-Polymer Composites. *Polymers*, **13**, 2375-2401. https://doi.org/10.3390/polym13142375

[7] Shtepliuk, I., Giannazzo, F. and Yakimova, R. (2021) Epitaxial Graphene on 4H-SiC (0001) as a Versatile Platform for Materials Growth: Mini-Review. *Applied Sciences*, **11**, 5784-5800. https://doi.org/10.3390/app11135784

[8] Kim, Y., Kim, Y. and Kim, J.H. (2020) Highly Conductive PEDOT: PSS Thin Films with Two-Dimensional Lamellar Stacked Multi-Layers. *Nanomaterials*, **10**, 2211-2220. https://doi.org/10.3390/nano10112211

[9] Chua, M.H., Zhu, Q., Shah, K.W. and Xu, J. (2019) Electroluminochromic Materials: From Molecules to Polymers. *Polymers*, **11**, 98-132. https://doi.org/10.3390/polym11010098

[10] Pu, Z., Zheng, P. and Zhang, Y. (2021) Poly(3,4-Ethylenedioxythiophene) (PEDOT) Nanofibers Decorated Graphene Oxide (GO) as High-Capacity, Long Cycle Anodes for Sodium Ion Batteries. *Materials*, **11**, 2032-2041. https://doi.org/10.3390/ma11102032

[11] Cymann, A., Sawczak, M., Ryl, J., Klugmann-Radziemska, E. and Wilamowska-Zawlocka, M. (2020) Capacitance Enhancement by Incorporation of Functionalised Carbon Nanotubes into Poly(3,4-Ethylenedioxythiophene)/Graphene Oxide Composites. *Materials*, **13**, 2419-2435. https://doi.org/10.3390/ma13102419

[12] Sharma, S., Sudhakara, P., Omran, A.A.B., Singh, J. and Ilyas, R.A. (2021) Recent Trends and Developments in Conducting Polymer Nanocomposites for Multifunctional Applications. *Polymers*, **13**, 2898-2928. https://doi.org/10.3390/polym13172898

[13] Dagadu, N.A., Ajori, S., Bensah, Y.D., Kan-Dapaah, K., Armah, S.K., Onwona-Agyeman, B. and Yaya, A. (2020) Stacking Interactions of Poly Para-Phenylene Vinylene Oligomers with Graphene and Single-Walled Carbon Nanotubes: A Molecular Dynamics Approach. *Molecules*, **25**, 4812-4835. https://doi.org/10.3390/molecules25204812

[14] Qazi, R.A., Khattak, R., Shah, L.A., Ullah, R., Khan, M.S., Sadiq, M., Hessien, M.M. and El-Bahy, Z.M. (2021) Effect of MWCNTs Functionalization on Thermal, Electrical, and Ammonia-Sensing Properties of MWCNTs/PMMA and PHB/MWCNTs/PMMA Thin Films Nanocomposites. *Nanomaterials*, **11**, 2625-2646. https://doi.org/10.3390/nano11102625

[15] Poldsalu, I., Rohtlaid, K., Plesse, C., Vidal, F., Nguyen, N.T., Peikolainen, A.L., Tamm, T. and Kiefer, R. (2020) Printed PEDOT:PSS Trilayer: Mechanism Evaluation and Application in Energy Storage. *Materials*, **13**, 491-513. https://doi.org/10.3390/ma13020491

[16] Rouway, M., Natchtane, M., Tarfaoui, M., Chakhchaoui, N., Omari, L.H., Fraija, F. and Cherkaoui, O. (2021) Mechanical Properties of a Biocomposite Based on Carbon Nanotube and Graphene Nanoplatelet Reinforced Polymers: Analytical and Numerical Study. *Journal of Composites Science*, **5**, 234-245. https://doi.org/10.3390/jcs5090234

[17] Joo, H., Han, H. and Cho, S. (2021) Fabrication of Poly(vinyl alcohol)-Polyaniline Nanofiber/Graphene Hydrogel for High-Performance Coin Cell Supercapacitor. *Polymers*, **12**, 928-943. https://doi.org/10.3390/polym12040928

[18] Kumar, V., Kumar, A., Lee, D. and Park, S. (2021) Estimation of Number of Graphene Layers Using Different Methods: A Focused Review. *Materials*, **14**, 4590-4611. https://doi.org/10.3390/ma14164590

[19] Wu, S., Tao, X. and Xu, W. (2021) Thermal Conductivity of Poplar Wood Veneer

Impregnated with Graphene/Polyvinyl Alcohol. *Forests*, **12**, 777-791. https://doi.org/10.3390/f12060777

[20] Guo, S., Chen, J., Zhang, Y. and Liu, J. (2021) Graphene-Based Films: Fabrication, Interfacial Modification, and Applications. *Nanomaterials*, **11**, 2539-2558. https://doi.org/10.3390/nano11102539

[21] Sui, S., Wang, Y., Dimitrakopoulos, C. and Perry, S.L. (2018) A Graphene-Based Microfluidic Platform for Electrocrystallization and *in Situ* X-Ray Diffraction. *Crystals*, **8**, 76-87. https://doi.org/10.3390/cryst8020076

[22] Sahu, D., Sutar, H., Senapati, P., Murmu, R. and Roy, D. (2021) Graphene, Graphene-Derivatives and Composites: Fundamentals, Synthesis Approaches to Applications. *Journal of Composites Science*, **5**, 181-210. https://doi.org/10.3390/jcs5070181

[23] Peng, C. and Zhang, X. (2021) Chemical Functionalization of Graphene Nanoplatelets with Hydroxyl, Amino, and Carboxylic Terminal Groups. *Chemistry*, **3**, 873-888. https://doi.org/10.3390/chemistry3030064

[24] Yang, Y., Palencia, J.L.D., Wang, N., Jaing, Y. and Wang, D. (2021) Nanocarbon-Based Flame Retardant Polymer Nanocomposites. *Molecules*, **26**, 4670-4701. https://doi.org/10.3390/molecules26154670

[25] Bokare, A., Arif, J. and Erogbogbo, F. (2021) Strategies for Incorporating Graphene Oxides and Quantum Dots into Photoresponsive Azobenzenes for Photonics and Thermal Applications. *Nanomaterials*, **11**, 2211-2250. https://doi.org/10.3390/nano11092211

[26] Luceno-Sanchez, J.A., Diez-Pascual, A.M. and Capilla, R.P. (2019) Materials for Photovoltaics: State of Art and Recent Developments. *International Journal of Molecular Sciences*, **20**, 976-1017. https://doi.org/10.3390/ijms20040976

[27] Wand, J., Adami, D., Lu, Bo., Liu, C., Maazouz, A. and Lamnawar, K. (2020) Multiscale Structural Evolution and Its Relationship to Dielectric Properties of Micro-/Nano-Layer Coextruded PVDF-HFP/PC Films. *Polymer*, **12**, 2596-2607. https://doi.org/10.3390/polym12112596

[28] Jiang, Y., Deng, Y. and Qi, J. (2021) Microstructure Dependence of Output Performance in Flexible PVDF Piezoelectric Nanogenerators. *Sensors and Actuators B: Polymer*, **13**, 3252-3262. https://doi.org/10.3390/polym13193252

[29] Shamsuri, A.A., Daik, R. and Jamil, S.N.A.M. (2021) A Succinct Review on the PVDF/Imidazolium-Based Ionic Liquid Blends and Composites: Preparations, Properties, and Applications. *Processes*, **9**, 761-827. https://doi.org/10.3390/pr9050761

[30] Zhao, H., Jiang, J. and Shi, M. (2021) Electrodeposition of Aluminum in the 1-Ethyl-3-Methylimidazolium Tetrachloroaluminate Ionic Liquid. *Electrochem*, **2**, 185-196. https://doi.org/10.3390/electrochem2020013

[31] Dzulkipli, M.Z., Karim, J., Ahmad, A., Dzulkurnain, N.A., Suait, M.S., Yoshizawa-Fujita, M., Khoo, L.T. and Hassan, N.H. (2021) The Influences of 1-Butyl-3-Methylimidazolium Tetrafluoroborate on Electrochemical, Thermal and Structural Studies as Ionic Liquid Gel Polymer Electrolyte. *Polymers*, **13**, 1277-1293. https://doi.org/10.3390/polym13081277

[32] Ray, A. and Saruhan, B. (2021) Application of Ionic Liquids for Batteries and Supercapacitors. *Materials*, **14**, 2942-2962. https://doi.org/10.3390/ma14112942

[33] Kim, E., Han, J., Ryu, S., Choi, Y. and Yoo, J. (2021) Ionic Liquid Electrolytes for Electrochemical Energy Storage Devices. *Materials*, **14**, 4000-4030. https://doi.org/10.3390/ma14144000

[34] Rahman, Md.H., Werth, H., Goldman, A., Hida, Y., Diesner, C., Lane, L. and Menezes, P.L. (2021) Recent Progress on Electroactive Polymers: Synthesis, Properties and Applications. *Ceramics*, **4**, 516-541. https://doi.org/10.3390/ceramics4030038

[35] Rauber, D., Hofmann, A., Phillipi, F., Kay, C.W.M., Zinkevich, T., Hanemann, T. and Hempelann, R. (2021) Structure-Property Relation of Trimethyl Ammonium Ionic Liquids for Battery Applications. *Applied Sciences*, **11**, 5679-5702. https://doi.org/10.3390/app11125679

[36] El Seoud, O.A., Keppelr, N., Malek, N.I. and Galgano, P.D. (2021) Ionic Liquid-Based Surfactants: Recent Advances in Their Syntheses, Solution Properties, and Applications. *Polymers*, **13**, 1100-1150. https://doi.org/10.3390/polym13071100

[37] Conway, B.E. (1999) Electrochemical Supercapacitors: Scientific Fundamentals and Technological Applications. Kluwer Academics and Plenum, New York.

[38] Cheng, Z. and Xu, C. (2021) Thermal Stability of Ionic Liquids: Current Status and Prospects for Future Development. *Processes*, **9**, 337-372. https://doi.org/10.3390/pr9020337

[39] Jiang, K. and Gerhardt, R.A. (2021) Fabrication and Supercapacitor Applications of Multiwall Carbon Nanotube Thin Films. *Journal of Carbon Research*, **7**, 70-141. https://doi.org/10.3390/c7040070